Journal of Materials Science: Materials in Electronics (2018) 29:16478–16485
https://doi.org/10.1007/s10854-018-9741-5

Hierarchical porous nitrogen-doped carbon material for high performance sodium ion batteries

Junke Ou[1] · Lin Yang[2] · Zhen Zhang[2]

Received: 25 April 2018 / Accepted: 24 July 2018 / Published online: 25 July 2018

Abstract
Hierarchical porous carbon materials (HPCMs) with appropriate nitrogen doping have been successfully fabricated from the gelatin by KOH activation. The HPCMs contain porous structure with suitable nitrogen content (2.85%), which specific surface area reach up to 1006 $m^2 g^{-1}$. When applied as anode materials for sodium ion batteries, the HPCMs deliver superior electrochemical performances, including a favorable reversible capacity of 261 mAh g^{-1} at the current density of 100 mA g^{-1}, excellent rate performance (104 mAh g^{-1} at 5 A g^{-1}), and superior cycling capability (220 mAh g^{-1} at 100 mA g^{-1} after 100 cycles).

1 Introduction

Due to abundant and environmental benignity of sodium source, sodium ion batteries (SIBs) have been recognized as the most potential new battery for the energy storage devices [1, 2]. In recent years, various cathode materials have been reported to show considerable progress for the development of SIBs [3–6]. However, the development of corresponding negative electrode materials for SIBs has been relatively slow.

As we know, due to their good conductivity, low price and environmental benignity, carbon-based materials have been considered as anode materials for SIBs. An effective approach of accelerating Na^+ diffusion is to shorten the diffusion pathways of Na^+ in the electrode materials. Especially the porous carbon, can not only facilitate sodium ion transport by reducing the diffusion lengths but also raise the contact areas between the electrode and electrolyte, which are both beneficial for the improvement of the electrochemical properties [7–10]. Moreover, modification with non-carbon atoms (particularly the N atom), is another effective mean to improve the electrochemical property of carbonaceous materials as the anode for sodium ion batteries [11–15]. Therefore, for the carbonaceous anode materials in SIBs, porous structure and incorporation of nitrogen are both desirable for Na^+ storage. Some works about biomass-derived carbons inspired us to develop cheap and high-performance carbon materials for energy-storage applications [16–19].

In this work, a facile strategy was reported to fabricate porous carbon, which shows high surface area and appropriate N doping. Gelatin with inherent N content, is derived from leathers and animal bones has been employed as a raw material. KOH was selected as a porogen to produce pore structure. After KOH activation, hierarchical porous carbon materials (HPCMs) with suitable nitrogen doping were fabricated. Because of the unique hierarchical porous structure and suitable nitrogen doping, the as-obtained HPCMs delivers high capacity and excellent rate capability, exhibiting a favorable reversible capacity as high as 220 mAh g^{-1} at 100 mA g^{-1} after 100 cycles. Compared with the previous works for preparing heteroatoms doped porous carbon, this work has several advantages: (1) gelatin is inherently rich in nitrogen (without any extra N source predecessor), which is an ideal precursor for nitrogen doping carbon materials; (2) compared to the template synthesis methods (such as SiO_2 template method, which involves the toxic HF solution), this preparation process is simple and facile, which makes it suitable for mass production; and (3) the as-obtained carbons show superior electrochemical performances for SIBs.

✉ Junke Ou
ojk0002@126.com

[1] Institute for Advanced Study, Chengdu University, Shiling Town, Chengdu 610106, China

[2] School of Basic Medical Sciences & Nursing, Chengdu University, Shiling Town, Chengdu 610106, China

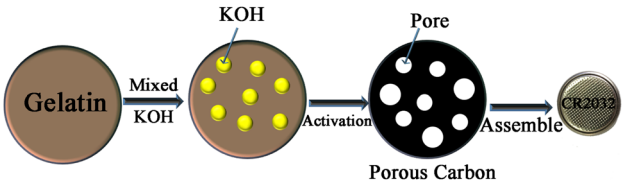

Fig. 1 Illustration of preparation of hierarchical porous carbon material

2 Experimental sections

2.1 Preparation of HPCMs

HPCMs were fabricated by chemical activation of gelatin (as illustrated in Fig. 1). Typically, gelatin and KOH was mixed (weight ratio, gelatin: KOH = 1:3), fired to 700 °C with a heat ramping rate of 5 °C min^{-1} and calcined for 1 h in argon. The obtained composite was then washed with 1 M hydrochloric acid solution and distilled water until pH became neutral. The carbon was finally dried in an oven at 70 °C. The yield of this process was around 30%. For comparison, the direct carbonized gelatin without KOH treatment was denoted as N-HPCMs.

2.2 Characterization

The transmission electron microscopy (TEM) images were made applying a FEI Tecnai G2 20. XRD patterns of the samples were carried out on a Bruker Powder X-Ray Diffractometer. The Raman spectrum was carried out using a confocal LabRAM HR800 spectrometer, HORIBA Jobin Yvon, France. Nitrogen adsorption/desorption analysis was conducted with an automatic analyzer (Autosorb-IQ, USA). XPS spectra were characterized using a Kratos XSAM 800 spectrometer (Manchester, UK). Electrochemical impedance spectroscopy (EIS) spectra were obtained by the CHI650e between the frequency of 0.01 and 100 KHz.

2.3 Electrochemical test

The electrochemical performance of the fabricated HPCMs was tested in 2032-coin cells. Na metal was applied as anode, 1 M $NaClO_4$ in a mixture of dimethyl carbonate (DMC) and ethylene carbonate (EC) (1:1, v/v) as electrolyte, and Celgard 2400 as separator. The HPCMs active material was mixed with acetylene black (AB) and polyvinylidene fluoride (PVDF) binder with a weight ratio of 8:1:1 in the *N*-methyl pyrrolidinone (NMP) solvent. The electrode was made by coasting the slurry onto a Cu foil and then drying at 120 °C for 5 h. The galvanostatic charge/discharge tests were conducted between 0.01 and 2.8 V versus Na^+/Na on a Newware CT-3008W battery cycler (Guangdong, China). Cyclic voltammetry (CV) was tested by a CHI650e electrochemical workstation in the range of 0.01–2.8 V versus Na^+/Na at a scan rate of 0.1 mV s^{-1}.

3 Results and discussion

Figure 2a displays the XRD pattern of the obtained carbon sample after KOH treatment at 700 °C and being washed with HCl solution. Two peaks located at 23.6° and 43.6° can be attributed to the (002) and (100) reflections of graphitic carbon, respectively, suggesting the amorphous feature of the as-obtained carbon. Furthermore, a high intensity at (002) peak indicated that the as-obtained carbon showed a high crystallinity. According to the (002) peak, the value of $d_{(002)}$ spacing was calculated to be 0.376 by Bragg's formula. The large $d_{(002)}$ spacing may be favorable to the insertion and extraction of sodium ion during the charge/discharge process

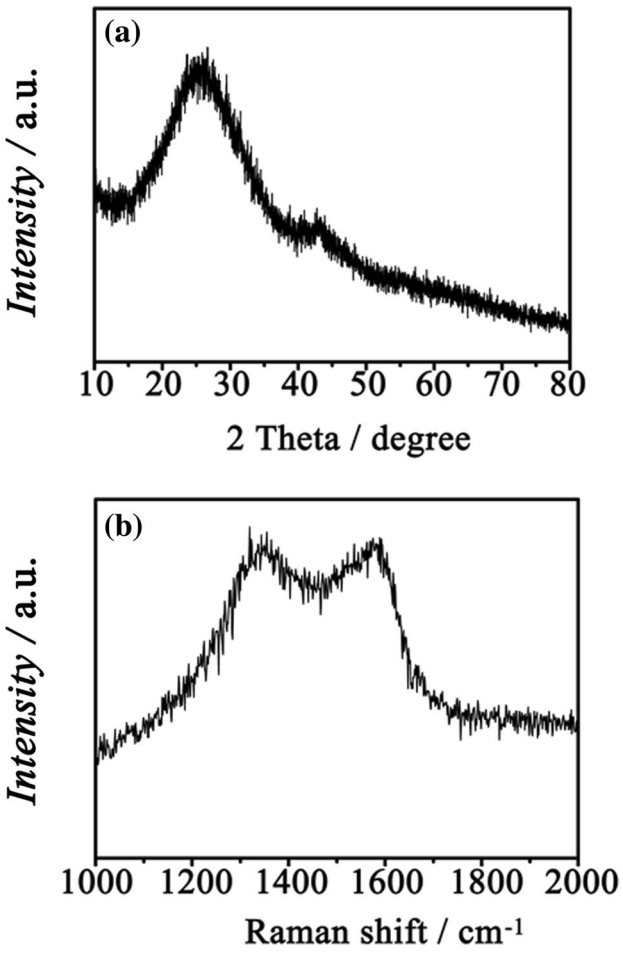

Fig. 2 **a** XRD pattern and **b** Raman spectra of the as-synthesized HPCMs

[20, 21]. The Raman spectrum of HPCMs (Fig. 2b) exhibits a G-band at 1592 cm^{-1} (related to graphitic carbon) and a D-band at 1359 cm^{-1} (associated with defects). Generally, the value of I_D/I_G is commonly applied to determine the graphitization of carbon materials. In this case, The I_D/I_G value of HPCMs is estimated to be 0.92, demonstrating a highly amorphous structure of the HPCMs, which can be agreed with the XRD result. The disordered structure may be more beneficial for reversible storage of the Na-ion [12, 22, 23].

The morphology of the gelatin-derived porous carbons is displayed in Fig. 3. As depicted in Fig. 3a (red arrow represents some mesopores), b, the TEM and HRTEM images clearly show that the as-obtained carbon delivers a hierarchical pore structure [micro- and mesopores (marked by the red arrow)]. This unique pore structure may originate from the KOH activation during the high temperature and is different from the single pore structure, which may derive from the template of SiO_2, MgO and $CaCO_3$ [24–26]. To further determine the porosity of the HPCMs, the nitrogen adsorption/desorption isotherm was carried out and shown in Fig. 3c. The N_2 adsorption/desorption isotherms show a much higher N_2 sorption capacity at a low relative pressure (P/P_0, range from 0 to 0.1), revealing a microporous property. With the increase of the relative pressure, the sorption capacity tends to be smooth, which indicate that the as-obtained HPCMs possess a hierarchical porous structure (micro- and mesopores). Furthermore, a large specific surface area of 1006 $m^2\ g^{-1}$ can be obtained, which is much higher than that of N-HPCMs (32 $m^2\ g^{-1}$). According to the TEM and N_2 adsorption/desorption isotherm, the carbon with micro-, mesopore and high specific surface area can provide a large electrode/electrolyte interface for ion or charge accumulation and facilitate the electrolyte penetration for sodium ion storage [27, 28]. The pore size distribution of the HPCMs is calculated applying the conventional density functional theory (DFT) method on the N_2 adsorption isotherm part as presented in Fig. 3d. The open system integrated a well-developed micro- and mesopore size distribution in the HPCMs. The total pore volume of HPCMs is found to be 0.54 $cm^3\ g^{-1}$ (micropore volume was 0.39 $cm^3\ g^{-1}$ and the mesopore volume was 0.16 $cm^3\ g^{-1}$) and the average pore size diameter 4.3 nm. Various pore

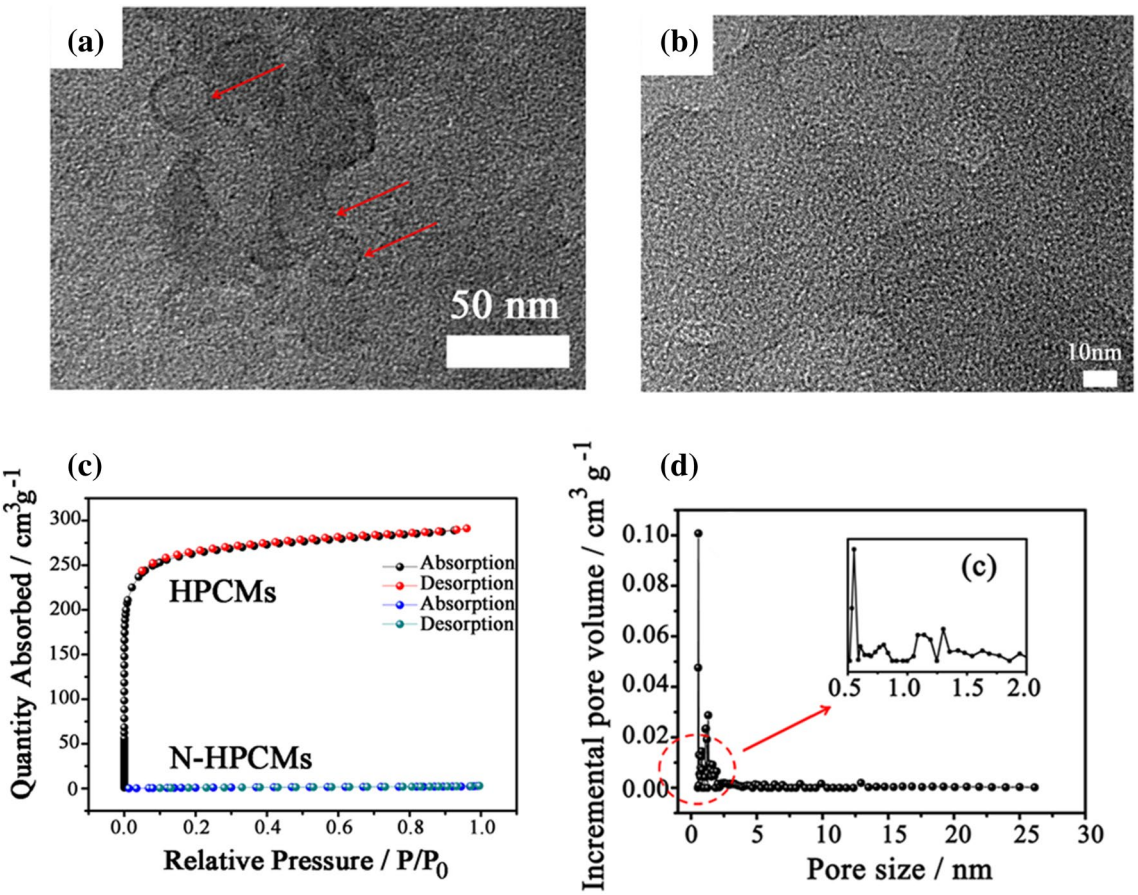

Fig. 3 TEM (**a**), HRTEM (**b**), nitrogen adsorption/desorption isotherm (**c**), pore size distribution (**d**) and enlarged micropore size distribution (**e**) of the obtained HPCMs

structures may play different roles in the transportation of the ions. The mesopores can act as reservoirs for storing electrolyte, resulting in reduced ion diffusion resistance and rapid ion transfer pathways. Large amount of micropores were favorable for the diffusion of sodium-ion and electrolyte in the carbon materials. This hierarchical pore structure (consisting of micropores and mesopores) could offer an effective path for penetration and transportation of electrolyte ions [29–31]. Such carbon with a unique hierarchical pore structure and a high surface area is expected to be a superior anode material for SIBs.

In order to evaluate the chemical states of the elements in the as-obtained carbons, XPS measurements are performed and displayed in Fig. 4. As presented in Fig. 4a, for the survey spectrum, the as-prepared HPCMs delivers three peaks located at 284.8, 400.0 and 533.6 eV, which related to C 1s, N 1s and O 1s, respectively. The calculated N content was about 2.85%. The high-resolution C 1s spectra (Fig. 4b) can be fitted by three peaks, located at 284.8 eV due to the graphitic (sp2 hybridized) carbon, at 286.1 eV corresponds to the carbons on the C–N and at 288.8 eV attributes to carbon on the C=O bonds. The N 1s spectrum (Fig. 4c) can be deconvoluted into two peaks, located at 398.3 and 400.7, respectively, which are attributed to two nitrogen components, namely, pyrrolic (N-5) and pyridinic (N-6) (as displayed in Fig. 4d), respectively. Furthermore, the oxygen, which mainly originated from the thermally stable functional groups of the carbon, was calculated to be about 9.35%, resulting in the enhancement of capacity by surface redox reactions ($–C=O + Na^+ + e \rightarrow –C–O–Na$) [32, 33]. According to the literatures [34, 35], N atoms at different positions in the carbon play different roles and affect the electrochemical performance of the as-fabricated carbon in different ways. The pyrrolic and pyridinic nitrogen atoms seated at the verge of the graphene layer, are beneficial for adsorbing exotic atoms and improving the sodium ions storage [36, 37]. Meanwhile, the N doping can increase the interlayer distance and the electrochemical activity of porous carbon, which offer more active sites for sodium ion storage [38]. Therefore, nitrogen doping in the carbon would be expected to offer more active sites for Na-ion storage, not just contributing to increase the electric conductivity of the material.

The electrochemical performance of the as-achieved carbons was carried out by cyclic voltammetric (CV) method at a scan rate of 0.5 mV s^{-1} between 0.01 and 2.8 V (vs. Na/Na^+). Figure 5a displays the CV profiles of the carbon electrode the first several cycles. In the first reduction process, the peak located at about 0.7 V is ascribed to the electrolyte

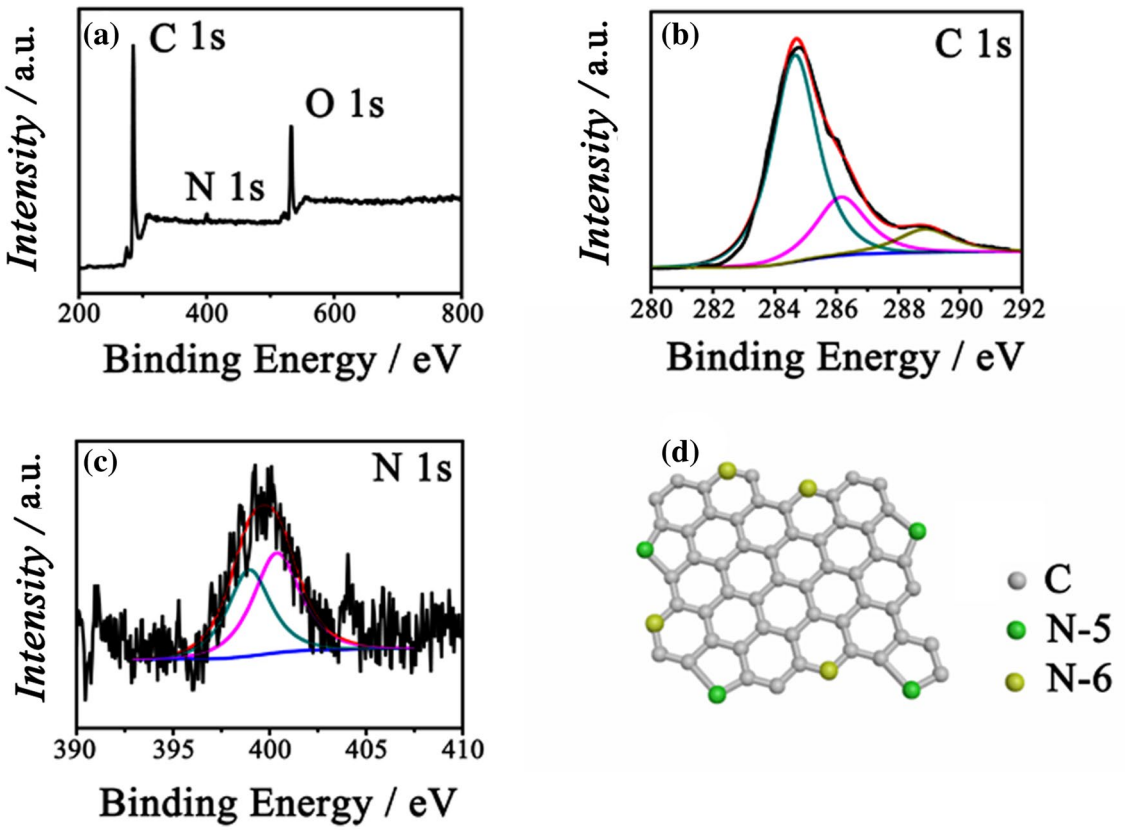

Fig. 4 **a** XPS total spectrum, **b** C 1s, **c** N 1s and **d** schematic structure of the binding conditions of nitrogen of HPCMs

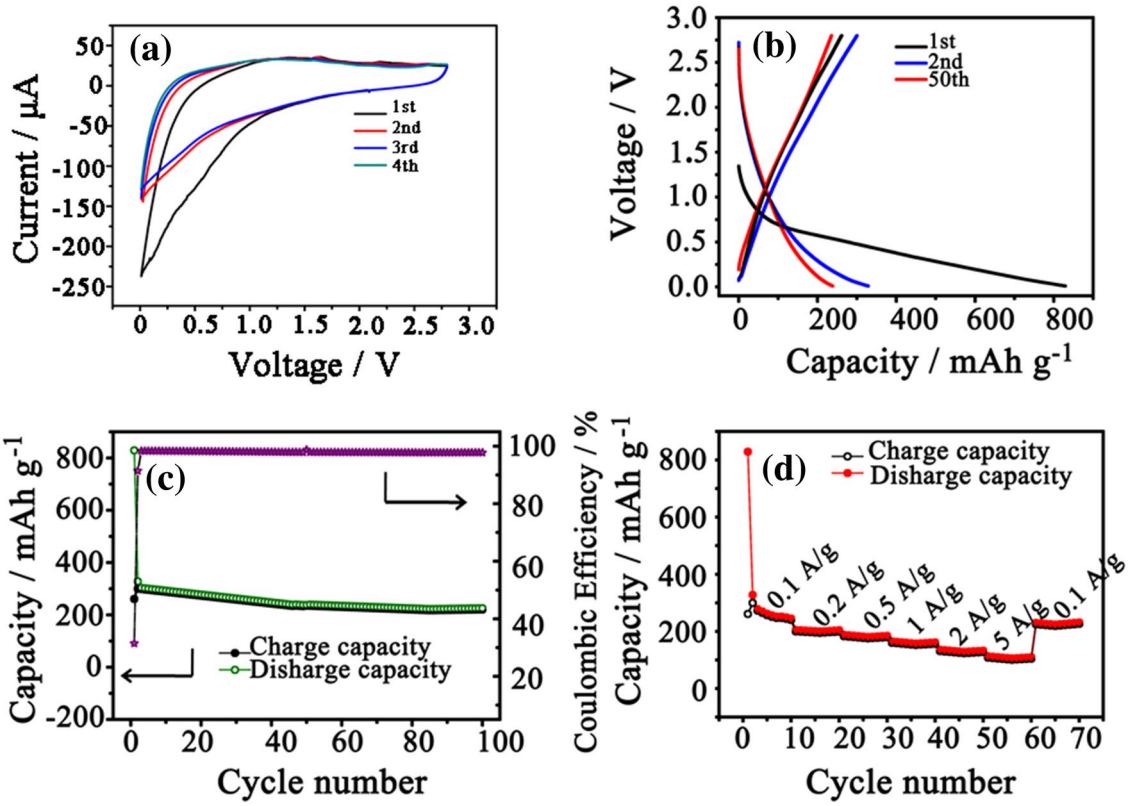

Fig. 5 **a** CV curve, **b** galvanostatic discharge/charge profile, **c** cycling performance and **d** rate performance of as-obtained HPCMs

decomposition and generation of a solid electrolyte interphase (SEI) film, which disappeared in the following cycles, suggesting a good reversibility of the carbons [39]. After the first scan, the second and following CV profiles almost overlap, suggesting good cycle property of HPCMs during Na^+ insertion and extraction. Figure 5b displays the charge/discharge profiles of the as-obtained HPCMs within 0.01–2.8 V, at the current density of 100 mA g^{-1}. The first charge/discharge cycle indicates the initial discharge and charge capacities to be 829 and 261 mAh g^{-1}, respectively, delivering an initial coulombic efficiency of 31.4%. The large irreversible capacity loss may result from the irreversible reaction between Na-ion and surface functional groups as well as with the electrolyte generating a SEI film [40, 41]. After the first cycle, the as-obtained carbons show exhibit good reversibility (236 mAh g^{-1} after 50 cycles). Once a stable SEI film is formed during the first cycle, the coulombic efficiency quickly reaches up to ca. 100% in the following cycles (Fig. 5c). As seen in Fig. 5c, the carbon delivers a favorable capacity of 220 mAh g^{-1} at 100 mA g^{-1} even after 100 cycles. Furthermore, as shown in Fig. 5d, the carbon shows superior rate capability. In detail, the carbon can deliver reversible capacities of 240, 199, 179, 156, 127 and 104 mAh g^{-1} at the current densities of 100, 200, 500, 1000, 2000, and 5000 mA g^{-1}, respectively. When it reduced back to 100 mA g^{-1}, the reversible capacity can recover to 226 mAh g^{-1}. Meanwhile, the SEM image and electrochemical performance of the direct carbonized gelatin can be seen in the Fig. 6. As shown in Fig. 6a, the N-HPCMs show a smooth surface, indicating a nonporous characteristic (which is in conformity with the result of the Fig. 3c). Figure 6b displays the electrochemical performance of the N-HPCMs at the current density of 0.1 A g^{-1} between 0.01 and 2.8 V. Specifically, the carbon shows capacities of 161, 150, 142 and 121 mAh g^{-1} at 1st, 2nd, 10th and 30th cycle, respectively. The electrochemical performance of the N-HPCMs was inferior to that of HPCMs, mainly derived from the large specific surface area of carbon material. This superior performance may be derived from the hierarchical porous structure and suitable N doping effects. First, the porous structure with a high surface area can facilitate the penetration of the electrolyte into the carbon electrode and ensure a reduced sodium ion diffusion pathway for rapid charge transport. Second, the suitable nitrogen doping can provide extra sites for Na-ion storage, thus further enhancing its rate-performance.

In order to investigate the kinetics of sodium ions in electrode, EIS analysis was conducted and displayed in Fig. 7. EIS spectra were obtained during the various charge/discharge cycles (the current density was 0.1 A g^{-1}). The low

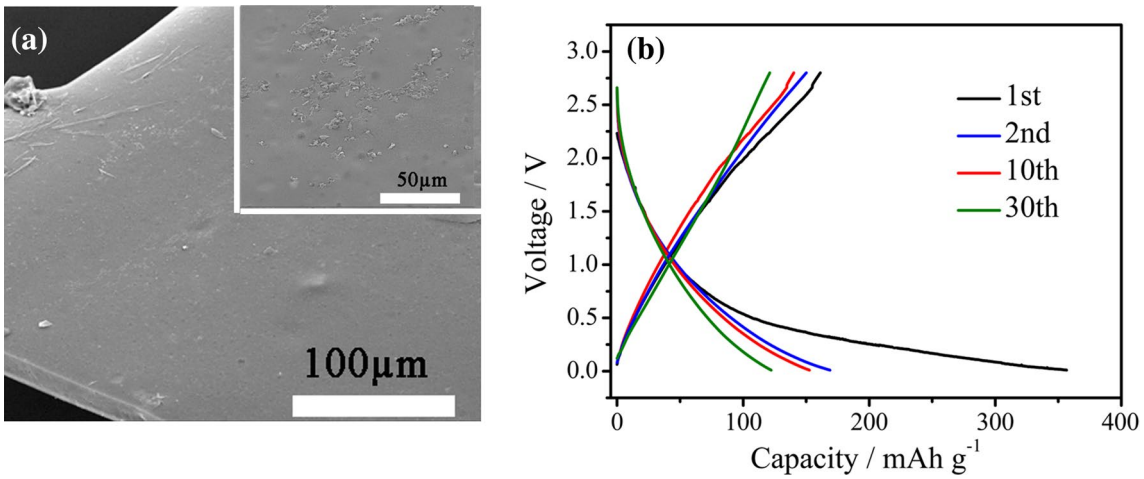

Fig. 6 SEM image (**a**) and charge/discharge profiles (**b**) (between 0.1 A g^{-1} in 0.01–2.8 V) of the N-HPCMs

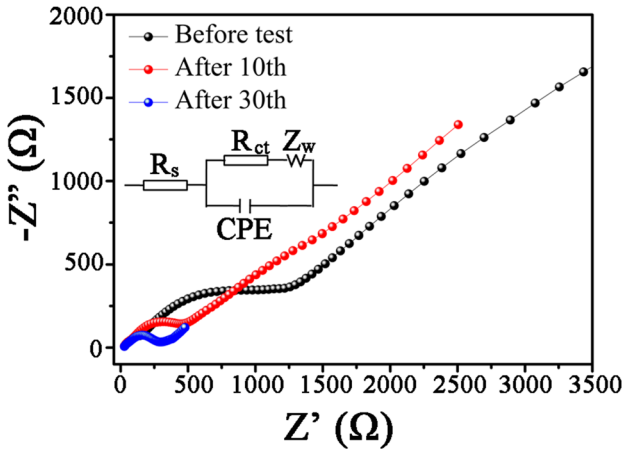

Fig. 7 EIS spectra of the HPCMs electrode in the before test, 10th and 30th (the current density was 0.1 A g^{-1})

frequency region showed a straight line, suggesting a Warburg element (Z_w) [42]. Higher frequencies delivered two features: R_s, indicative of resistance of electrode materials and contact resistance between the electrode and electrolyte; R_{ct}, referring to the charge transfer resistance [43]. After fitted by the equivalent circuit (as shown in the inset of Fig. 7), the R_s and R_{ct} of the carbon electrode in the before test, 10th and 30th were 202 and 1285 Ω, 67 and 496 Ω and 46 and 243 Ω, respectively. This result indicating the improved charge transfer with the increase of the cycling, this may be due to the activation of the electrode during the repeated sodium-ion insertion and extraction processes.

A comparison of the rate performance of HPCMs with several carbons reported in literature is also shown in Table 1. It can be clearly seen that the as-prepared HPCMs shows a much higher reversible capacity and better rate

Table 1 Electrochemical property comparison of HPCMs versus anode carbons of SIBs reported in literature

Sample	Initial reversible capacity (mAh g^{-1})	Cycle capability (mAh g^{-1})	References
HPCMs	261 at 0.1 A g^{-1}	220 after 100 cycles	This work
Templated carbon	180 at 0.0744 A g^{-1}	130 after 40 cycles	[44]
Hollow carbon nanospheres	223 at 0.05 A g^{-1}	160 after 100 cycles	[45]
Sphere carbon	160 at 0.15 A g^{-1}	90 after 50 cycles	[46]
Mesoporous carbon	160 at 0.1 A g^{-1}	125 after 100 cycles	[47]
Graphene oxide doped hard carbon	289 at 0.02 A g^{-1}	220 after 200 cycles	[48]
Nitrogen-doped porous hollow carbon spheres	175 at 0.2 A g^{-1}	120 after 100 cycles	[49]
Nitrogen-doped bamboo-like carbon nanotubes	167 at 0.1 A g^{-1}	110 after 160 cycles	[37]
Carbon fiber	255 at 0.04 A g^{-1}	176 after 200 cycles	[50]
Hollow carbon nanowires	251 at 0.05 A g^{-1}	251 after 400 cycles	[51]

capability at high current densities. The improved electrochemical performances of the gelatin-based carbons can be attributed to the unique hierarchical pore structure and appropriate N doping effects. More specifically, the material with large surface area delivers a reduced Na^+ diffusion pathway and a high electrode/electrolyte contact area, which can be beneficial to facilitate sodium ion diffusion and ultimately improve rate performance. Meanwhile, the unique porous structure can provide enough space to accommodate volume changes that result in superior cycling performance. Furthermore, suitable nitrogen doping can produce a large amount of defects in the carbon and form an amorphous structure, which further improves sodium absorption performances.

4 Conclusions

In summary, HPCMs were successfully fabricated from gelatin via a facile approach of KOH activation. Thanks to the unique hierarchical porous structure and appropriate N doping, the HPCMs as anode for sodium ion batteries (SIBs) deliver large reversible capacity (261 mAh g^{-1} at 100 mA g^{-1}), superior cycling durability (220 mAh g^{-1} at 100 mA g^{-1} after 100 cycles), and good rate performance (104 mAh g^{-1} at 5 A g^{-1}). Considering their excellent electrochemical performances and the facile preparation approach, HPCMs should be regarded as one of the most potential candidates as anode material for SIBs.

Acknowledgements We greatly appreciate the National Natural Science Foundation of China (No. 21606024) and Chengdu University new faculty start-up funding (No. 208191503) for supporting this work.

References

1. N. Yabuuchi, K. Kubota, M. Dahbi, S. Komaba, Research development on sodium-ion batteries. Chem. Rev. **114**, 11636–11682 (2014)
2. X. Ge, Z. Li, L. Yin, Metal-organic frameworks derived porous core/shellCoP@ C polyhedrons anchored on 3D reduced graphene oxide networks as anode for sodium-ion battery. Nano Energy **32**, 117–124 (2017)
3. A.R. Radwan, Y. Liu, V. Nguyen et al., Sodium vanadate nanoflowers/rGO composite as a high-rate cathode material for sodium-ion batteries. J. Mater. Sci.: Mater. Electron. **29**, 7032–7039 (2018)
4. Z. Jian, L. Zhao, H. Pan, Y.S. Hu, H. Li, W. Chen, L. Chen, Carbon coated $Na_3V_2(PO_4)_3$ as novel electrode material for sodium ion batteries. Electrochem. Commun. **14**, 86–89 (2012)
5. O.H. Han, J.K. Jung, M.Y. Yi, J.H. Kwak, Y.J. Shin, Sodium ion dynamics in the nonstoichiometric layer-type oxide $Na_{0.67}Ni_{0.33}Ti_{0.67}O_2$ studied by 23 Na NMR. Solid State Commun. **117**, 65–68 (2000)
6. Y. Zhao, X. Cao, G. Fang, Y. Wang, H. Yang, S. Liang, A.Q. Pan, G.Z. Cao, Hierarchically carbon-coated $Na_3V_2(PO_4)_3$ nanoflakes for high-rate capability and ultralong cycle-life sodium ion batteries. Chem. Eng. J. **339**, 162–169 (2018)
7. X.Q. Yang, C. Wei, C.C. Sun, X.X. Li, Y. Chen, High performance anode of lithium-ion batteries derived from an advanced carbonaceous porous network. J. Alloy Compd. **693**, 777–781 (2017)
8. F.C. Zheng, D. Liu, G.L. Xia, Y. Yang, T. Liu, M.Z. Wu, Q.W. Chen, Biomass waste inspired nitrogen-doped porous carbon materials as high-performance anode for lithium-ion batteries. J. Alloy Compd. **693**, 1197–1204 (2017)
9. D. Zhou, Y. Liu, W.L. Song, X.G. Li, L.Z. Fan, Y.H. Deng, Three-dimensional porous carbon-coated graphene composite as high-stable and long-life anode for sodium-ion batteries. Chem. Eng. J. **316**, 645–654 (2017)
10. P. Lu, Y. Sun, H. Xiang, X. Liang, Y. Yu, 3D amorphous carbon with controlled porous and disordered structures as a high-rate anode material for sodium-ion batteries. Adv. Energy Mater. **8**, 1702434 (2018)
11. J. Ou, L. Yang, Z. Zhang, X. Xi, Nitrogen-doped porous carbon derived from horn as an advanced anode material for sodium ion batteries. Microporous Mesoporous Mater. **237**, 23–30 (2017)
12. K.L. Hong, L. Qie, R. Zeng, Z.Q. Yi, W. Zhang, D. Wang, W. Yin, C. Wu, Q.J. Fan, W.X. Zhang, Y.H. Huang, Biomass derived hard carbon used as a high performance anode material for sodium ion batteries. J. Mater. Chem. A **2**, 12733–12738 (2014)
13. X. Yue, N. Huang, Z. Jiang, X. Tian, Z. Wang, X. Hao, Z. Jiang, Nitrogen-rich graphene hollow microspheres as anode materials for sodium-ion batteries with super-high cycling and rate performance. Carbon **130**, 574–583 (2018)
14. G. Zeng, B. Zhou, L. Yi, H. Li, X. Hu, Y. Li, Green and facile fabrication of hierarchical N-doped porous carbon from water hyacinths for high performance lithium/sodium ion batteries. Sustain. Energy Fuels **2**, 855–861 (2018)
15. C. Yang, J. Xiong, X. Ou, C. Wu, X. Xiong, J. Wang, K. Huang, M. Liu, A renewable natural cotton derived and nitrogen/sulfur co-doped carbon as a high-performance sodium ion battery anode. Mater. Today Energy **8**, 37–44 (2018)
16. C. Wang, Y. Xiong, H. Wang, N. Yang, C. Jin, Q. Sun, "Pickles method" inspired tomato derived hierarchical porous carbon for high-performance and safer capacitive output. J. Electrochem. Soc. **165**, A1054–A1063 (2018)
17. Q. Jiang, S. Zhang, S. Yin, Z. Guo, S. Wang, C. Feng, Biomass carbon micro/nano-structures derived from ramie fibers and corncobs as anode materials for lithium-ion and sodium-ion batteries. Appl. Surf. Sci. **379**, 73–82 (2016)
18. C. Yu, H. Hou, X. Liu, Y. Yao, Q. Liao, Z. Dai, D. Li, Old-loofah-derived hard carbon for long cyclicity anode in sodium ion battery. Int. J. Hydrog. Energy **43**, 3253–3260 (2018)
19. Q. Wang, X. Zhu, Y. Liu, Y. Fang, X. Zhou, J. Bao, Rice husk-derived hard carbons as high-performance anode materials for sodium-ion batteries. Carbon **127**, 658–666 (2018)
20. C. Wang, J. Huang, H. Qi, L. Cao, Z. Xu, Y. Cheng, X. Zhao, J. Li, Controlling pseudographtic domain dimension of dandelion derived biomass carbon for excellent sodium-ion storage. J. Power Sources **358**, 85–92 (2017)
21. Y. Sun, J. Tang, K. Zhang, J. Yuan, J. Li, D. Zhu, K. Ozawa, L. Qin, Comparison of reduction products from graphite oxide and graphene oxide for anode applications in lithium-ion batteries and sodium-ion batteries. Nanoscale **9**, 2585–2595 (2017)
22. J. Zhu, C. Chen, Y. Lu, Y. Ge, H. Jiang, K. Fu, X. Zhang, Nitrogen-doped carbon nanofibers derived from polyacrylonitrile for use as anode material in sodium-ion batteries. Carbon **94**, 189–195 (2015)
23. N. Sinan, E. Unur, Hydrothermal conversion of lignocellulosic biomass into high-value energy storage materials. J. Energy Chem. **26**, 783–789 (2017)

24. Y.S. Hu, P. Adelhelm, B.M. Smarsly, S. Hore, M. Antonietti, J. Maier, Synthesis of hierarchically porous carbon monoliths with highly ordered microstructure and their application in rechargeable lithium batteries with high-rate capability. Adv. Funct. Mater. **17**, 1873–1878 (2007)
25. C. Zhu, T. Akiyama, Cotton derived porous carbon via an MgO template method for high performance lithium ion battery anodes. Green Chem. **18**, 2106–2114 (2016)
26. Y. Mao, H. Duan, B. Xu, L. Zhang, Y. Hu, C. Zhao, Z.X. Wang, L.Q. Chen, Y. Yang, Lithium storage in nitrogen-rich mesoporous carbon materials. Energy Environ. Sci. **5**, 7950–7955 (2012)
27. J. Xiang, W. Lv, C. Mu, J. Zhao, B. Wang, Activated hard carbon from orange peel for lithium/sodium ion battery anode with long cycle life. J. Alloy Compd. **701**, 870–874 (2017)
28. N.A. Kaskhedikar, J. Maier, Lithium storage in carbon nanostructures. Adv. Mater. **21**, 2664–2680 (2009)
29. C. Wang, Y. Xiong, H. Wang, C. Jin, Q. Sun, Naturally three-dimensional laminated porous carbon network structured short nano-chains bridging nanospheres for energy storage. J. Mater. Chem. A **5**, 15759–15770 (2017)
30. H. Wang, C. Wang, Y. Xiong, C. Jin, Q. Sun, Simple synthesis of N-doped interconnected porous carbon from Chinese tofu for high-performance supercapacitor and lithium-ion battery applications. J. Electrochem. Soc. **164**, A3832–A3839 (2017)
31. H. Wang, C. Sheng, T. Cai, C. Jin, Q. Sun, Mesopore-dominant nitrogen-doped carbon with a large defect degree and high conductivity via inherent hydroxyapatite-induced self-activation for lithium-ion batteries. RSC Adv. **8**, 12204–12210 (2018)
32. M. Lu, W. Yu, J. Shi, W. Liu, S. Chen, X. Wang, H. Wang, Self-doped carbon architectures with heteroatoms containing nitrogen, oxygen and sulfur as high-performance anodes for lithium-and sodium-ion batteries. Electrochim. Acta **251**, 396–406 (2017)
33. Y. Shao, J. Xiao, W. Wang, M. Engelhard, X. Chen, Z. Nie, M. Gu, L.V. Saraf, G. Exarhos, J.G. Zhang, J. Liu, Surface-driven sodium ion energy storage in nanocellular carbon foams. Nano Lett. **13**, 3909–3914 (2013)
34. Y.C. Wang, B.Y. Zhu, J.F. Ni, L. Zhang, H.B. Wang, L.J. Gao, Pyrolyzed polyaniline-graphene nanosheets with enhanced lithium-storage properties: preparation and characterization. ChemElectroChem **1**, 951–956 (2014)
35. J. Machnikowski, B. Grzyb, J.V. Weber, E. Frackowiak, J.N. Rouzaud, F. Béguin, Structural and electrochemical characterisation of nitrogen enriched carbons produced by the co-pyrolysis of coal-tar pitch with polyacrylonitrile. Electrochim. Acta **49**, 423–432 (2004)
36. Z. Guan, H. Liu, B. Xu, X. Hao, Z. Wang, L. Chen, Gelatin-pyrolyzed mesoporous carbon as a high-performance sodium-storage material. J. Mater. Chem. A **3**, 7849–7854 (2015)
37. D. Li, L. Zhang, H. Chen, L.X. Ding, S. Wang, H. Wang, Nitrogen-doped bamboo-like carbon nanotubes: promising anode materials for sodium-ion batteries. Chem. Commun. **51**, 16045–16048 (2015)
38. H. Tao, L. Xiong, S. Du, Y. Zhang, X. Yang, L. Zhang, Interwoven N and P dual-doped hollow carbon fibers/graphitic carbon nitride: an ultrahigh capacity and rate anode for Li and Na ion batteries. Carbon **122**, 54–63 (2017)
39. L. Fu, K. Tang, K. Song, P.A. van Aken, Y. Yu, J. Maier, Nitrogen doped porous carbon fibres as anode materials for sodium ion batteries with excellent rate performance. Nanoscale **6**, 1384–1389 (2014)
40. Y.X. Wang, S.L. Chou, H.K. Liu, S.X. Dou, Reduced graphene oxide with superior cycling stability and rate capability for sodium storage. Carbon **57**, 202–208 (2013)
41. H.G. Wang, Z. Wu, F.L. Meng, D.L. Ma, X.L. Huang, L.M. Wang, X.B. Zhang, Nitrogen-doped porous carbon nanosheets as low-cost, high-performance anode material for sodium-ion batteries. ChemSusChem **6**, 56–60 (2013)
42. F. Zhang, T. Liu, G. Hou, T. Kou, L. Yue, R. Guan, Y. Li, Hierarchically porous carbon foams for electric double layer capacitors. Nano Res. **9**, 2875–2888 (2016)
43. Y. Gong, D. Li, C. Luo, Q. Fu, C. Pan, Highly porous graphitic biomass carbon as advanced electrode materials for supercapacitors. Green Chem. **19**, 4132–4140 (2017)
44. S. Wenzel, T. Hara, J. Janek, P. Adelhelm, Room-temperature sodium-ion batteries: improving the rate capability of carbon anode materials by templating strategies. Energy Environ. Sci. **4**, 3342–3345 (2011)
45. K. Tang, L. Fu, R.J. White, L. Yu, M.M. Titirici, M. Antonietti, J. Maier, Hollow carbon nanospheres with superior rate capability for sodium-based batteries. Adv. Energy Mater. **2**, 873–877 (2012)
46. V.G. Pol, E. Lee, D. Zhou, F. Dogan, J.M. Calderon-Moreno, C.S. Johnson, Spherical carbon as a new high-rate anode for sodium-ion batteries. Electrochim. Acta **127**, 61–67 (2014)
47. J. Liu, H. Liu, T. Yang, G. Wang, M.O. Tade, Mesoporous carbon with large pores as anode for Na-ion batteries. Chin. Sci. Bull. **59**, 2186–2190 (2014)
48. W. Luo, C. Bommier, Z. Jian, X. Li, R. Carter, S. Vail, Y. Lu, J. Lee, X. Ji, Low-surface-area hard carbon anode for Na-ion batteries via graphene oxide as a dehydration agent. ACS Appl. Mater. Interfaces **7**, 2626–2631 (2015)
49. K. Zhang, X. Li, J. Liang, Y. Zhu, L. Hu, Q. Cheng, C. Guo, N. Lin, Y. Qian, Nitrogen-doped porous interconnected double-shelled hollow carbon spheres with high capacity for lithium ion batteries and sodium ion batteries. Electrochim. Acta **155**, 174–182 (2015)
50. W. Luo, J. Schardt, C. Bommier, B. Wang, J. Razink, J. Simonsen, X. Ji, Carbon nanofibers derived from cellulose nanofibers as a long-life anode material for rechargeable sodium-ion batteries. J. Mater. Chem. A **1**, 10662–10666 (2013)
51. Y. Cao, L. Xiao, M.L. Sushko, W. Wang, B. Schwenzer, J. Xiao, Z. Nie, L. Saraf, Z. Yang, J. Liu, Sodium ion insertion in hollow carbon nanowires for battery applications. Nano Lett. **12**, 3783–3787 (2012)